THE JOURNAL OF PHYSICAL CHEMISTRY B

Article

pubs.acs.org/JPCB

Elastic Properties of Nanoparticle Monolayer Foams

Uli Langer, Ayan Ray, Saeedeh Aliaskarisohi, and Thomas M. Fischer*

Lehrstuhl für Experimentalphysik V, Universität Bayreuth, Bayreuth, Germany

Supporting Information

ABSTRACT: Monolayers of nanosized carboxylate-functionalized polystyrene particles at the air/water interface assemble into two coexisting liquid phases of different densities. The rheological properties of the individual phases and of the resulting nanoparticle texture is measured using a magnetic needle microrheometer. We show that, despite the liquid behavior of the individual viscous phases, the entire structure exhibits elastic response to local deformations induced by the needle. We explain this response by microscopically nonresolved nanofacets that connect the domains and form a two-dimensional foam.

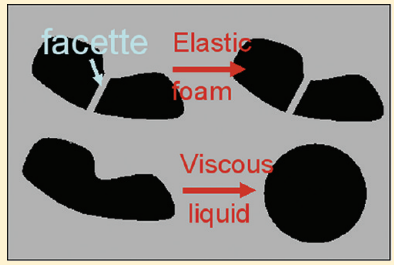

INTRODUCTION

Colloidal suspensions build complex fluids that play a role in our daily life. Paint is a colloidal suspension that is of low viscosity when applied and is highly viscous after drying. The amount of red blood cells in our blood dominates the flow properties of blood in our body. Colloids of particular interest are particles that assemble at an interface between two liquids via the Pickering effect.[1−3] Such two-dimensional colloidal suspensions lead to the formation of interfacial complex fluids with interfacial rheological properties.[4] They strongly depend on the surface concentration of entrapped beads at the interface. It has been shown by Ruiz-Garcia[5] that micrometer-sized particles at the air/water interface arrange into superstructures consisting of more and less dense regions of particles. Hence they very much resemble the behavior of ordinary insoluble surfactants where a rich variety of differently ordered Langmuir monolayer phases[6] are formed as a function of temperature. Langmuir monolayers of surfactant molecules behave like viscous liquids in the less dense liquid expanded phases, but also exhibit viscoelastic behavior at larger surfactant densities.[7,8] The field of interfacial rheology originally based on investigations using macroscopic interfacial rheometers[9] has received a boost in recent years through the development of new microrheological techniques.[10−14] They allow one to measure viscous properties of interfaces in a regime not accessible to macroscopic measurements. In this work we show by the use of a magnetic needle interfacial microrheometer[12] that interfacial viscoelastic response in a nanoparticle interfacial assembly arises not from the properties of the individual coexisting particle phases but from the mesoscopic foamlike texture of the phase coexistence region. In our work, we first give a brief description of our monolayer preparation and the needle rheometer; second we show that both coexisting nanoparticle phases are purely viscous liquids. The viscosities of each of the phases is determined quantitatively, and the line tension between both phases is determined. Then we show that the response of mesoscopic structures is viscoelastic. The forces that act on persisting mesoscopic structures are quantified for one example. These forces are explained by postulating the existence of nonresolved nanofacets that connect the individual domains and form a two-dimensional foam.

MATERIALS AND METHODS

We spread fluorescent carboxylate-modified microspheres of diameter $2a = 0.1\ \mu$m (Invitrogen F8801 from Sigma Aldrich) from acetone onto a nanopure water subphase (Siemens LaboStar 7, 18MΩ/cm) in a Teflon trough. By the use of a fluorescence microscope (Leica DM 2500 MH), we visualize the resulting nanoparticle monolayers. The magnetic nickel microneedles for the magnetic deformation of the monolayer are produced by electrodeposition of nickel into a nanoporous membrane (Nucleopore Track-Etch Membrane PC MB 25MM 0.03 from Whatman) from which we extract the resulting nickel needles and coat them with fluorescent dye (Invitrogen Alexa Fluor 488). The electrodeposition procedure closely follows the recipe described by Bentley et al.[15] We coat the upper side of the nanoporous membrane (Nucleopore Track-Etch Membrane PC MB 25MM 0.03 μm from Whatman) with galium indium eutectic (Ga−In eutectic >99.99% trace metals basis from Aldrich). We attach the coated membrane to a copper plate with an electric tape so that the coated side of the membrane looks down toward the copper electrode. Except for the surface of the membrane, the copper plate is electrically isolated. We connect the negative lead of a power supply to the copper plate and the positive lead to a nickel wire (0.5 mm diam., 99.9 + % metals basis from Sigma-Aldrich). We place both in a beaker filled with high speed nickel sulfamate FFP electrolyte. We adjust the power supply to 1.5 and an initial current of 20 mA. Electrolysis is done for 40 min for the desired length ($l = 12\ \mu$m) of the nickel rods. Afterward, we remove the copper plate from the beaker and place it in acetone (99.9% from Sigma-Aldrich) to remove the electrical tape. By the use of

Received: February 8, 2012
Revised: May 9, 2012
Published: May 14, 2012

   dx.doi.org/10.1021/jp301278j | J. Phys. Chem. B 2012, 116, 6439−6442

concentrated nitric acid (65% from Sigma-Aldrich) we remove the gallium indium coating and rinse the membrane with water several times to reach a neutral pH. We place the membrane in 1 mL of 2 M NaOH (from Sigma-Aldrich) solution for 30 min to dissolve it. We attract the nickel rods left behind with a strong magnet and remove the NaOH solution. Then we wash the extracted nickel rods repeatedly with nanopure water until a neutral pH is reached. To fluorescently label these rods, we remove the water and directly apply Alexa Fluor 488 (from Invitrogen) to them. We keep the rods in the solvent for 2 h before we transfer them to an acetone solution in which they are stored until usage. The nickle rods are spread onto the subphase before the nanoparticles. The microrheological setup is similar to the one described by Dhar et al.[12] Two pairs of coils are placed perpendicular to each other (Figure 1) around

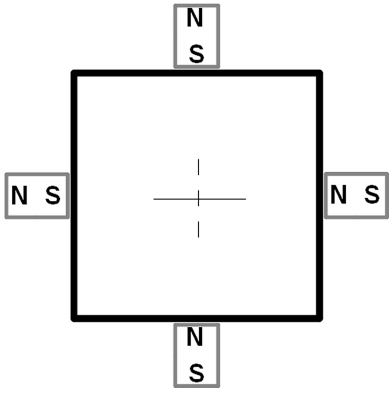

Figure 1. Schematic drawing of the micro needle rheometer. Two pairs of magnetic coils are surrounding the trough. The magnetic field is alternated between the *x*- and the *y*-directions, and the shearing of the monolayer due to the reorientation of the micro needle is observed with fluorescence microscopy.

the trough to allow a switching of the magnetic field into two directions. Videos of the nanoparticle monolayer and the magnetic needles were captured via the fluorescence microscope at 39.5 frames per second using a digital high-speed camera (DFC 360FX from Leica) mounted onto the microscope. The videos were stored digitally in a computer for further analysis. Individual frames were extracted from the video file using virtualdub (v.1.9.11, http://www.virtualdub.org). Image analysis was performed using standard procedures in ImageJ (v.1.45p, http://rsbweb.nih.gov/ij/).

RESULTS

In Figure 2 we show the texture of a nanoparticle monolayer at an average surface density of 32 particles/μm^2 consisting of a low- and high-density phase of particles arranged in a domain-like fashion. Different microrheological experiments are used to reveal the rheological properties of the individual phases. In the denser phase, we observe a vigorous Brownian motion of the nanoparticles. In Figure 3 we depict the mean square displacement of the particles as a function of time. We see a linear increase of the mean square displacement $(\Delta x)^2(t)$ according to

$$(\Delta x)^2(t) = 4Dt \tag{1}$$

from which we extract a diffusion constant of $D = 0.65\ \mu$m^2/s. The diffusion of a sphere of radius a on the air−water surface of viscosity η in a homogeneous phase of surface shear viscosity η_s

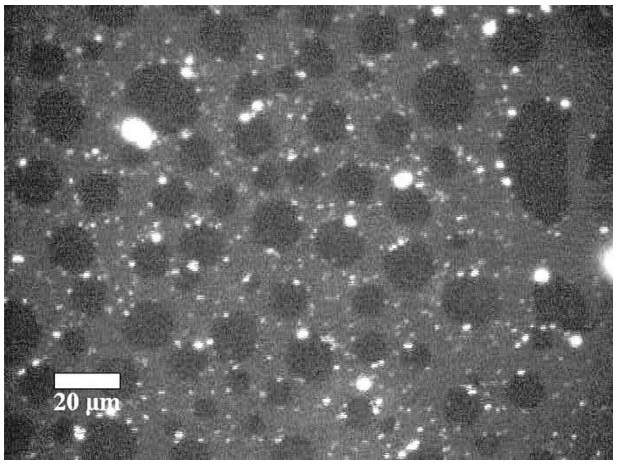

Figure 2. Fluorescence microscopy image of the coexistence region between a low and high nanoparticle density phase on the air/water interface.

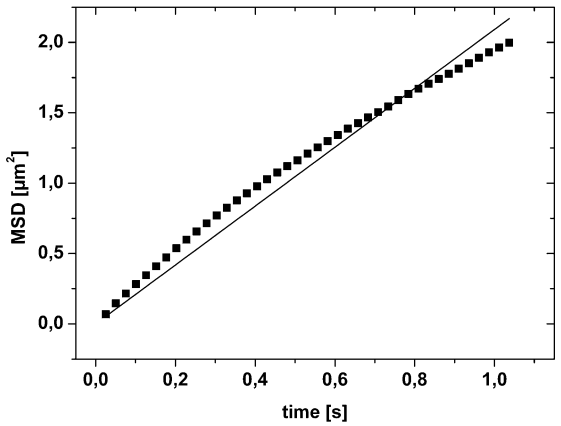

Figure 3. Mean square displacement of one nanoparticle in the high density phase as a function of time. The straight line corresponds to a linear fit according to eq 1 with a diffusion constant of $D = (0.52 \pm 0.02)\mu$m^2/s. The value of $(D = 0.65 \pm 0.5)\mu$m^2/s is obtained by taking the average over 11 particles.

has been analyzed theoretically by Fischer et al.[16] In their treatment, the diffusion constant can be written as

$$D = \frac{k_B T}{f\eta a} \tag{2}$$

where k_B is Boltzmann's constant and T is the temperature. The parameter f is a friction coefficient depending on the relative immersion of the bead into the water and on the ratio $\eta_s/\eta a$. Our diffusion constant of the beads in the denser phase corresponds to a friction coefficient $f \approx 124.4$. Assuming a half immersion of the beads into the subphase, this corresponds to a viscous two-dimensional liquid behavior of the denser phase of viscosity $\eta_s \approx 0.39$ nNs/m. Experiments with the microneedle rheometer also reveal the liquid behavior of the less dense phase. If we switch the direction of the magnetic field, we observe the rotation of the magnetic needles by 90°. Upon rotation, the needles distort the monolayer texture. In Figure 4 we show a distorted low-density domain that relaxes to a circular shape after the switch. The relaxation of weakly deformed domains back to a circular shape have been described theoretically by Stone et al.[17] and by Mann et al.[18] by

dx.doi.org/10.1021/jp301278j | J. Phys. Chem. B 2012, 116, 6439−6442

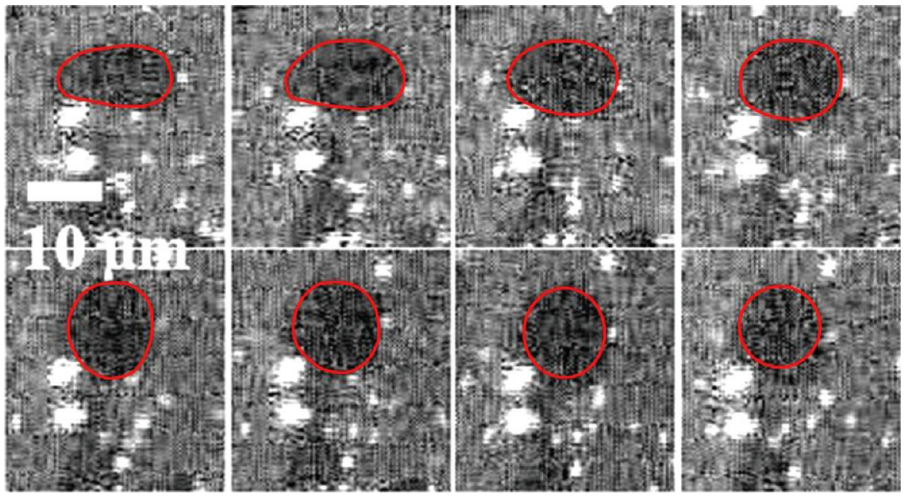

Figure 4. Relaxation of a low density domain occurring after distortion of the monolayer with the magnetic micro needle. The time between two images is 126 ms.

decomposing the time-dependent radial coordinates of the domain shape $r(\varphi)$ into Fourier modes:

$$r(\varphi) = R + \sum_n \varepsilon_n(t) \cos(n(\varphi - \varphi_n)) \tag{3}$$

where R is the radius of the relaxed circular domain, and $\varepsilon_n(t)$ represents the time-dependent Fourier coefficients of the distorted shape that relax exponentially with rates Γ_n

$$\varepsilon_n(t) = \varepsilon_n(0)\mathrm{e}^{-\Gamma_n t} \tag{4}$$

The dominating dissipation governing the relaxation of the domain can be read off from the scaling of the relaxation rates with the size and the Fourier mode n of the distortion. If surface viscous dissipation dominates, the problem can be reduced to a purely two-dimensional one, and one finds[18]

$$\Gamma_n \propto R^{-1} \tag{5}$$

while for dissipation into the subphase one finds[17]

$$\Gamma_n = \frac{n^2 4(n^2 - 1)\lambda}{(4n^2 - 1)\eta\pi R^2} \tag{6}$$

Here λ denotes the line tension between the low- and high-density phase. The domain shapes in Figure 4 could be fitted reasonably well using only the second Fourier coefficient $\varepsilon_2(t)$. This Fourier coefficient is plotted in Figure 5 as a function of time for two differently sized low-density domains and fitted with an exponential decay (eq 4). For the domain with $R_1 = (5.6 \pm 0.1)$ μm, we fit a relaxation rate of $\Gamma_2^1 = (3.10 \pm 0.14)$ s^{-1} and a line tension of $\lambda = (95 \pm 4)$ fN, while for a domain with $R_2 = (13.8 \pm 0.1)$ μm we measure a relaxation rate of $\Gamma_2^2 = (0.51 \pm 0.01)$ s^{-1} and a line tension of $\lambda = (96 \pm 2)$ fN. The ratio of the relaxation rates is $\Gamma_2^1/\Gamma_2^2 = (6.06 \pm 0.30)$, which relates well to the ratio of the squared radii $(R_2/R_1)^2 = 6.12 \pm 0.24$. From this we confirm that surface viscosities are indeed negligible for both of the phases, and the phases can be considered to exhibit a pure liquid-like response to mechanical deformations. It is therefore surprising that the response of the larger scale texture is not completely viscous. In some circumstances when the magnetic needles deform the texture, the texture partially persists. Certain low-density domains do not relax to circular, but keep their shape as long as the magnetic needle is held in the distorted position. Only after switching the magnetic field and the needle back to the original orientation does the domain return to circular. A movie of this behavior can be observed in the Supporting Information. Partially elastic behavior of monolayer textures has been reported for liquid condensed phases by Ignés-Mullol et al.[19] It has been recently reported also for the liquid expanded/liquid condensed coexistence region of dipalmitoylphosphatidylcholine (DPPC) monolayers by Squires.[11] Squires et al. related the elastic response to elongated stripes of one phase connecting different domains of the other phase. Here we postulate the existence of low-density foam facets below the microscopic resolution that keep the liquid foam bubbles in their particular shape. Assuming that the rheological properties of the individual phases behave as determined above, we may use the Young Laplace equation for the domain shapes to locate the points on the distorted domains where excess forces act on the domain to keep it in its distorted shape. Figure 6 shows a persistent distorted low-density domain of perimeter $P = (142 \pm 10)$ μm that keeps its shape after the distortion. The mean curvature of the domain is $\overline{\kappa} = 2\pi/P$ such that the Laplace pressure is $\Delta\pi = \lambda\kappa$, with κ being the curvature of the domain at a particular point on the perimeter. The excess force density at

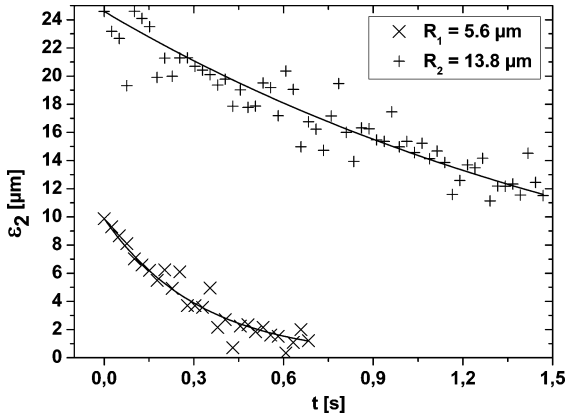

Figure 5. Plot of the second-order Fourier components ε_2 versus time of the deformation of two domains with $R_1 = (5.6 \pm 0.1)$ μm and $R_2 = (13.8 \pm 0.1)$ μm. Both Fourier coefficients decay exponentially with $\Gamma_2^1 = (3.10 \pm 0.14)$ s^{-1} and $\Gamma_2^2 = (0.51 \pm 0.01)$ s^{-1}.

dx.doi.org/10.1021/jp301278j | J. Phys. Chem. B 2012, 116, 6439−6442

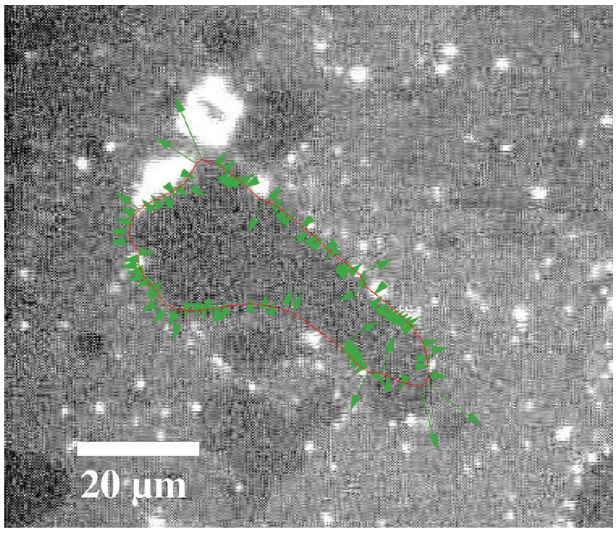

Figure 6. Fluorescence microscopy image of a persistently deformed domain. The red line shows the computed perimeter used to calculate the force density profile represented by the green arrows. A movie of the persistence of this domain after turning the magnetic needle can be viewed in the Supporting Information.

the perimeter of the domain keeping the domain in its particular shape is therefore given by

$$\vec{f}_{\text{ext}}(s) = (\kappa - \bar{\kappa})\vec{n} \tag{7}$$

In Figure 6 we have depicted the excess force density acting on the distorted domain. This force density exhibits peaks pointing outside and inside the domain at the positions where the curvature strongly deviates from the mean curvature. It is at these points that we postulate the existence of facets. Facets of the high-density phase are postulated to span from points where the excess force points inside the low density domain. Facets of the low-density phase should span toward the locations where the excess force is pointing outward from the domain. In this way, albeit all the constituents of the texture are liquid, the foam structure of the liquids would provide the elasticity observed that is typical for this texture and leads to the complex rheological behavior of structured fluids.

CONCLUSION

Nanoparticles at the air/water interface arrange in a coexistence of a low- and high-density phase that forms a foamlike structure with facets that lie below the microscopic resolution spanning between the domains. While the rheological behavior of individual domains can be described by a purely liquid behavior with negligible surface shear viscosity and a line tension between the phases of the order of 0.1 pN, the mesoscopic structure of the arrangement nevertheless gives rise to elastic response of the two-dimensional nanoparticle texture.

ASSOCIATED CONTENT

Supporting Information

Movie showing the rotation of the magnetic needle and the persistence of the distorted domain shape that only returns to circular after switching back the magnetic needle. This information is available free of charge via the Internet at http://pubs.acs.org.

AUTHOR INFORMATION

Corresponding Author

*E-mail: Thomas.Fischer@uni-bayreuth.de.

Notes

The authors declare no competing financial interest.

ACKNOWLEDGMENTS

Support of the German Science foundation via Grant Fi 548 11-1 is highly acknowledged.

REFERENCES

(1) Pickering, S. U. *J. Chem. Soc., Trans.* **1907**, *91*, 2001−2021.
(2) Pieranski, P. *Phys. Rev. Lett.* **1980**, *45*, 569−572.
(3) Ramsden, W. *Proc. R. Soc. London* **1903**, *72*, 156−164.
(4) Peng, Y.; Chen, W.; Fischer, T. M.; Weitz, D. A.; Tong, P. *J. Fluid Mech.* **2009**, *618*, 243−261.
(5) Ruiz-Garcia, J.; Gámez-Corrales, R.; Ivlev, B. I. *Phys. A (Amsterdam, Neth.)* **1997**, *236*, 97−104.
(6) Kaganer, V. M.; Möhwald, H.; Dutta, P. *Rev. Mod. Phys.* **1999**, *71*, 779−819.
(7) Fischer, B.; Tsao, M.-W.; Ruiz-Garcia, J.; Fischer, T.; Schwartz, D.; Knobler, C. *Thin Solid Films* **1996**, *284*−*285* (0), 110−114.
(8) Kim, K.; Choi, S. Q.; Zasadzinski, J. A.; Squires, T. M. *Soft Matter* **2011**, *7*, 7782−7789.
(9) Georgiadou, S.; Brooks, B. W. *Chem. Eng. Sci.* **2006**, *61*, 6892−6901.
(10) Benvegnu, D. J.; McConnell, H. M. *J. Phys. Chem.* **1992**, *96*, 6820−6824.
(11) Choi, S.; Steltenkamp, S.; Zasadzinski, J.; Squires, T. *Nat. Commun.* **2011**, *2*, 312:1−6.
(12) Dhar, P.; Cao, Y.; Fischer, T. M.; Zasadzinski, J. A. *Phys. Rev. Lett.* **2010**, *104*, 016001:1−4.
(13) Prasad, V.; Koehler, S. A.; Weeks, E. R. *Phys. Rev. Lett.* **2006**, *97*, 176001:1−4.
(14) Steffen, P.; Heinig, P.; Wurlitzer, S.; Khattari, Z.; Fischer, T. M. *J. Chem. Phys.* **2001**, *115*, 994−997.
(15) Bentley, A. K.; Farhoud, M.; Ellis, A. B.; Nickel, A.-M. L.; Lisensky, G. C.; Crone, W. C. *J. Chem. Educ.* **2005**, *82*, 765−768.
(16) Fischer, T. M.; Dhar, P.; Heinig, P. *J. Fluid Mech.* **2006**, *558*, 451−475.
(17) Stone, H. A.; McConnell, H. M. *Proc. R. Soc. London, Ser. A* **1995**, *448*, 97−111.
(18) Mann, E. K.; Hénon, S.; Langevin, D.; Meunier, J.; Léger, L. *Phys. Rev. E* **1995**, *51*, 5708−5720.
(19) Ignés-Mullol, J.; Schwartz, D. K. *Nature* **2001**, *410*, 348−351.